CrossMark

Synthesis and Properties of the $La_{1-x-y}Eu_yCa_xVO_4$ $(0 \leq x, y \leq 0.2)$ Compounds

O. V. Chukova[1*], S. G. Nedilko[1], A. A. Slepets[2], S. A. Nedilko[2] and T. A. Voitenko[2]

Abstract

The $La_{1-x}Ca_xVO_4$ and $La_{1-x-y}Eu_yCa_xVO_4$ $(0 \leq x, y \leq 0.2)$ micro/nanosized powders were prepared by aqueous nitrate–citrate sol–gel synthesis. Phase composition of the sample depends on the x and y values. The $La_{0.9}Ca_{0.1}VO_4$ is crystallized in monoclinic structure up to the $x = 0.1$. The $La_{0.9}Eu_{0.05}Ca_{0.05}VO_4$ sample was also attributed to the monoclinic structure. Increasing concentration of europium and calcium ions in $La_{1-x-y}Eu_yCa_xVO_4$ solid solutions leads to the change of the crystal structure, and subsequently, stabilization of the tetragonal phase takes place.

The obtained samples were characterized by XRD analysis, SEM microscopy, and IR spectroscopy. Luminescence properties of the synthesized powders were studied. Emission of the $La_{1-x}Ca_xVO_4$ samples is weak and consists of wide bands in the 450–800 nm spectral range. The observed bands at 570 and 630 were ascribed to electron transitions in the distorted VO_4^{3-} vanadate groups. Emission of the $La_{1-x-y}Eu_yCa_xVO_4$ samples consists of narrow spectral lines in the 550–730 nm spectral range. The lines are caused by the $^5D_0 \rightarrow {}^7F_J$ electron transitions in the Eu^{3+} ions. The Ca^{2+} ions incorporation increases the intensity of the Eu^{3+} ions luminescence. Structure of the spectra depends on Ca^{2+} concentration and excitation wave length. The carried out analysis has revealed that Eu^{3+} ions form at least two different types of emission centers in the $La_{1-x-y}Eu_yCa_xVO_4$ samples. The assumption is made that type I centers are formed by the Eu^{3+} ions in their regular positions in the crystal lattice, while the type II centers have complex structure and consist of Eu^{3+} ions, Ca^{2+} cations, and oxygen vacancies.

Keywords: Vanadate, Sol–gel, Eu^{3+}, Luminescence

Background

Rare earth orthovanadates are very interesting class of compounds which have very important applications in various fields involving chemistry and biology, luminescent nanoparticles, and light transformers [1–4]. Orthovanadates can exhibit unusual magnetic, optical, thermally activated, and X-ray luminescence properties [5]. Nanosized orthovanadates have also attracted considerable research interest as perspective photocatalyst systems for photocatalytic water splitting. The widely used photocatalyst TiO_2 is active only under ultraviolet light irradiation [1, 6], while europium ($EuVO_4$) [7] and lanthanum ($LaVO_4$) [8] orthovanadates are of a special attention as the most promising visible-light-driven photocatalysts [9]. These compounds are chemically stable and non-toxic [10, 11]. Their range of biological applications includes fluorescent probes for

single-molecule tracking, drug development, protein detection, and fluorescent bio labeling [2, 11, 12].

Actually, some of the abovementioned applications require vanadate materials with improved efficiency of luminescence excitation under light from near UV and violet spectral ranges [4, 13–15]. The search for new vanadate compounds for these needs is carried out using variations of two and more cations in their composition including partial iso- and heterovalent substitutions [16–19]. It was shown previously that intensities of luminescent emission of the RE activators in orthovanadate compounds can be effectively increased with the A^{2+} modifying cations (A = Ca, Sr, Ba, Pb, etc.) [4, 16, 20–22]. Moreover, properties of compositions with such heterovalent substitutions are strongly dependent on concentration ratios of the A^{2+} cations. Besides, our recent investigations have shown that increase of intensity of luminescence emission of rare earth orthovanadates can be also achieved with improvement of method of synthesis and morphology of the nanoparticles [14, 23]. Therefore, we expect that expansion of the best of

* Correspondence: chukova@univ.kiev.ua
[1]Faculty of Physics, Taras Shevchenko National University of Kyiv, 64/13, Volodymyrska Str, 01601 Kyiv, Ukraine
Full list of author information is available at the end of the article

Chukova *et al. Nanoscale Research Letters* (2017) 12:340

Page 2 of 11

our recent practices for synthesis of the rare earth orthovanadate nanaparticles onto the same compositions with heterovalent substitutions could bring an additional raise of emission intensity of luminescent orthovanadate nanoparticles. At the first step in this direction, we use the Ca^{2+} modifying impurities as the cheapest reagent.

The aim of this work is to study synthesis procedures, structural features, and morphological and optical characteristics of the nanosized $La_{1-x}Ca_xVO_4$ and $La_{1-x-y}Eu_yCa_xVO_4$ $(0 \leq x, y \leq 0.2)$ compounds. Various methods can be applied for synthesis of the orthovanadates nanoparticles, such as solid state [16, 23], hydrothermal [24], solution combustion [17], and sol–gel methods [14, 25]. One of the most promising ways to perform an excellent homogenization for nanoscale sizes of particles, high reactivity of the compounds, and morphology that satisfy enhanced emission intensity is the sol–gel method.

Methods/Experimental
Synthesis
The $La_{1-x}Ca_xVO_4$ and $La_{1-x-y}Eu_yCa_xVO_4$ samples $(0 \leq x, y \leq 0.2)$ were prepared by aqueous nitrate–citrate sol–gel synthesis route using citric acid (CA) as a complexing agent. Lanthanum (III) and europium (III) nitrates $La(NO_3)_3$ (99.0%, High Purity Chemicals), $Eu(NO_3)_3$ (99.0%, High Purity Chemicals), calcium (II) nitrate $Ca(NO_3)_2$ (99.0%, High Purity Chemicals), and ammonium metavanadate NH_4VO_3 (99.0%, High Purity Chemicals) were used as starting compounds. They were weighted according to the desired stoichiometric molar ratio. Nitric acid (HNO_3), distilled water, and ammonia ($NH_3 \cdot 4H_2O$) were used as solvents and reagents to regulate the pH of the solutions. Firstly, NH_4VO_3 was dissolved in concentrated ammonia solution by stirring at 70–80 °C temperature. Then, the CA dissolved in distilled water with a small amount of $NH_3 \cdot 4H_2O$ was

added. Next, $La(NO_3)_3$, $Eu(NO_3)_3$, and $Ca(NO_3)_2$ were added. To prevent precipitation, the pH that reached the value of ~6–7 was controlled. Finally, the same amount of the aqueous solution of the complexing agent CA was repeatedly added to the reaction mixture to prevent crystallization of metal salts during the gelation process. The clear solution was concentrated by slow evaporation at 80–90 °C in an open beaker. A transparent gel has been formed after evaporation of nearly 90% of the water during the continuous stirring. The powders were obtained after drying in an oven at 100 °C. The powders were step by step calcined for 5 h at the range from 150 to 700 °C. Figure 1 illustrates the process of synthesis.

Equipment
Phase compositions and crystal lattice parameters of the synthesized samples were determined using X-ray diffractometer DRON-3M (CuKα-radiation with a Ni filter). The diffraction patterns were taken with a 2°/min step. Characterization of the samples' morphology was made using scanning electron microscope (SEM) Tescan Mira 3 LMU with 20-nm electronic beam diameter. The secondary electron detector (InBeam) could be used, if there is a need, to enhance spatial resolution up to 1 nm. Infrared (IR) spectra of the samples were recorded on PerkinElmer IR spectrometer using the KBr pellet method in the 1400–400 cm^{-1} range. Luminescence spectra were measured at high resolution equipment using DFS-12 and DMR-23 diffraction spectrometers with excitation by diode lasers, nitrogen gas laser, and xenon lamp (see more details in [26, 27]).

Results and Discussion
X-ray Diffraction
The X-ray diffraction (XRD) patterns of the synthesized $La_{1-x}Ca_-VO_4$ and $La_{1-x-y}Eu_yCa_xVO_4$ $(x \leq 0.2, y \leq 0.2)$

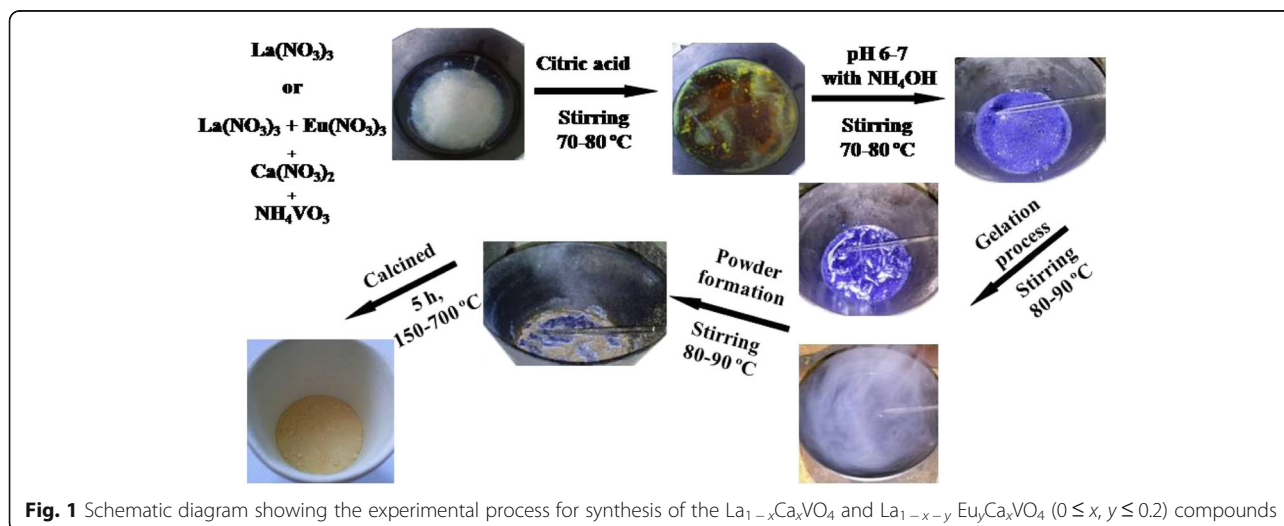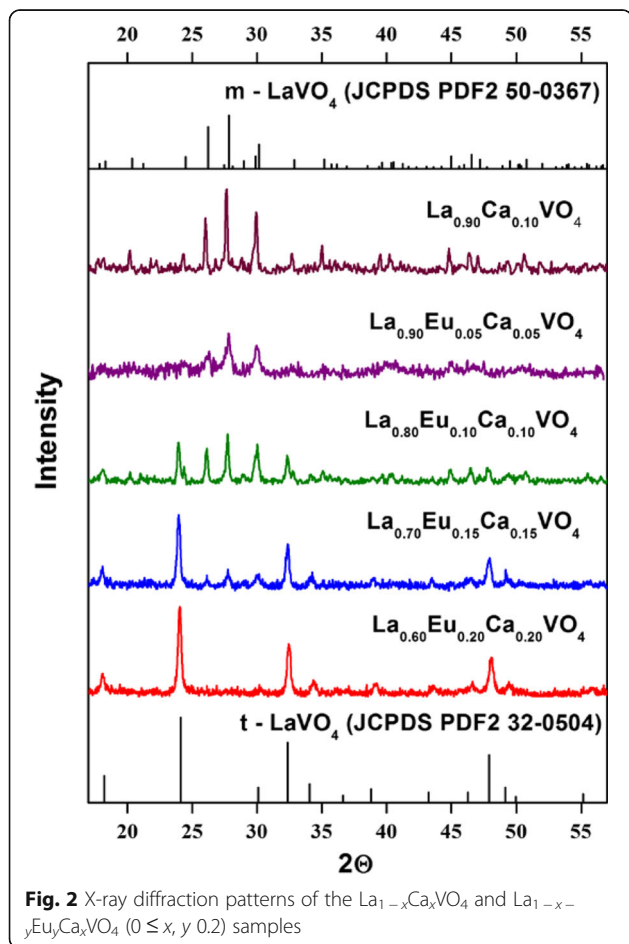**Fig. 1** Schematic diagram showing the experimental process for synthesis of the $La_{1-x}Ca_xVO_4$ and $La_{1-x-y}Eu_yCa_xVO_4$ $(0 \leq x, y \leq 0.2)$ compounds

Chukova *et al. Nanoscale Research Letters* (2017) 12:340

Page 3 of 11

samples are shown in Fig. 2. It was found that the $La_{0.9}Ca_{0.1}VO_4$ sample is crystallized in monoclinic structure; a space group is P2$_1$/n (see Fig. 2). This result is well matched with a standard card of monoclinic LaVO$_4$ (JCPDS PDF2 50-0367) (see Fig. 2). The $La_{0.9}Eu_{0.05}$-$Ca_{0.05}VO_4$ sample with low concentration of the Ca^{2+} and Eu^{3+} impurities is also attributed to the monoclinic structure. Proximity of the Ca^{2+} (1.12 nm), La^{3+} (1.16 nm), and Eu^{3+} (1.066 nm) ions radii provides an opportunity for calcium and europium ions' incorporation into three plus cation's sites. Besides, we see that small quantities of the Ca^{2+} ($x \leq 0.1$) and Eu^{3+} ions ($y \leq 0.05$) can enter to the crystal lattice without change of the monoclinic LaVO$_4$ structure.

Increasing concentrations of the Eu^{3+} and Ca^{2+} impurities leads to formation of the monoclinic and tetragonal phase mixture (Fig. 2). The $La_{0.6}Eu_{0.2}Ca_{0.2}VO_4$ sample becomes related to tetragonal structure, belonging to the I41/amd space group. This result is agreed with the standard card of tetragonal LaVO$_4$ (JCPDS PDF2 32-0504) (see Fig. 2). If some amount of the residual monoclinic phase is still presented in these samples, it was below the detection limit of our XRD equipment.

Fig. 2 X-ray diffraction patterns of the $La_{1-x}Ca_xVO_4$ and $La_{1-x-y}Eu_yCa_xVO_4$ ($0 \leq x, y$ 0.2) samples

Therefore, increasing concentration of europium and calcium ions in $La_{1-x-y}Eu_yCa_xVO_4$ ($x, y \leq 0.2$) solid solutions leads to the change of the crystal structure, and subsequently, stabilization of the tetragonal phase takes place.

Morphology and Chemical Element Analysis

The set of characteristic SEM images of the $La_{1-x-y}Eu_x$-Ca_yVO_4 samples are shown in Fig. 3. The top two images, a and b, show areas of ~5 × 5 μm; in other words, general view of samples is given, whereas other images, c–f, show small separated areas, up to ~0.5 × 0.5 μm size. It is easy to see from general view that samples consist of grains of different sizes, from tens of nanometers to 1 μm. Grains of large sizes (0.2–1.0 μm) are agglomerates of smaller ones, and they have no certain shapes. Detailed view of agglomerates and of small grains (Fig. 3c–f) show that they are formed by nanoparticles of size from 20 to 100 nm. The $La_{0.9}Eu_{0.05}Ca_{0.05}VO_4$ samples with low concentration of the Eu and Ca impurities consist of grains of 0.1–0.2 μm-size, those are formed by nanoparticles of 10–20-nm size (Fig. 3c). The nanoparticles of larger size, ~100 nm, are characteristic for the samples with higher concentration of dopants, $La_{0.8}Eu_{0.1}Ca_{0.1}VO_4$. Most of them have polyhedral shapes with clearly defined edges and angles between them (Fig. 3d). The particles with the observed polyhedral shapes have to be assigned to the crystal system of lower symmetry. Thus, most likely, they should be regarded as a manifestation of the monoclinic phase of the studied samples. The next increase of the Eu^{3+} and Ca^{2+} dopant concentrations also generates particles of ~100-nm sizes (Fig. 3e). Despite of the poor quality of this image, it is possible to conclude that the shapes of the particles are closer to the cylinders and rods. The same shapes are observed for the samples of the highest dopant concentration, $La_{0.6}Eu_{0.2}Ca_{0.2}VO_4$ (Fig. 3f). However, it should be noted that size of the particles is smaller for these samples; it is preferably 30–60 nm.

Thus, we can say that the change of the powder samples' composition is accompanied by the changes in the size and morphology of their constituent particles. These changes are consistent with the XRD data on the structure and phase composition of the samples. Therefore, the SEM data can be interpreted as indicating that the samples of higher dopant concentration are mixtures of monoclinic and tetragonal phases and the content of the latter increases when the content of europium and calcium ions increases.

Chemical element analysis was performed for 3–5 various agglomerates or grains for each sample using SEM tools. Monitoring area from which information about content of atoms have been taken was larger than e-beam size, and it was near (30–40) × (30–40) μm. We have found that La, Eu, Ca, V, and O are the main

Chukova *et al. Nanoscale Research Letters* (2017) 12:340
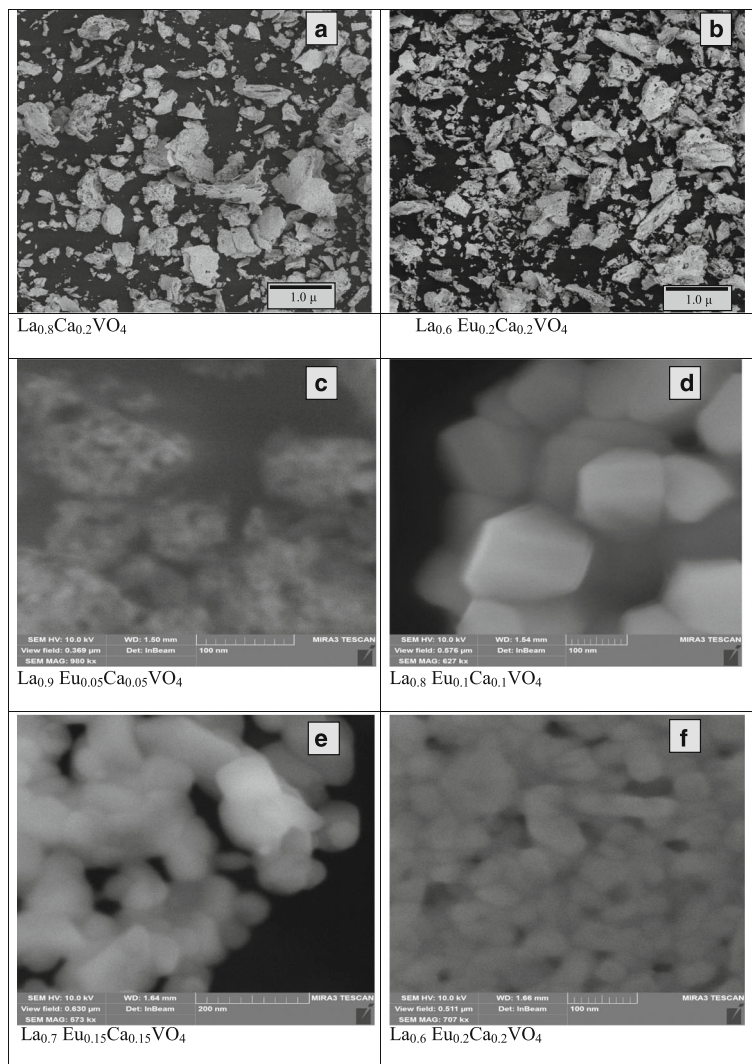
Page 4 of 11

Fig. 3 The SEM images of the La0.8Ca0.2VO4 (**a**), La0.6 Eu0.2Ca0.2VO4 (**b**, **f**), La0.9 Eu0.05Ca0.05VO4 (**c**), La0.8 Eu0.1Ca0.1VO4 (**d**), and La0.7 Eu0.15Ca0.15VO4 (**e**) samples

components of the samples. In certain cases, some quantity of carbon atoms revealed that obvious occurred when edge zone of grains or grains of small thickness were monitored. (Powder samples were fixed on special carbon-covered scotch tape for SEM measurements.) Average data are accumulated in Table 1.
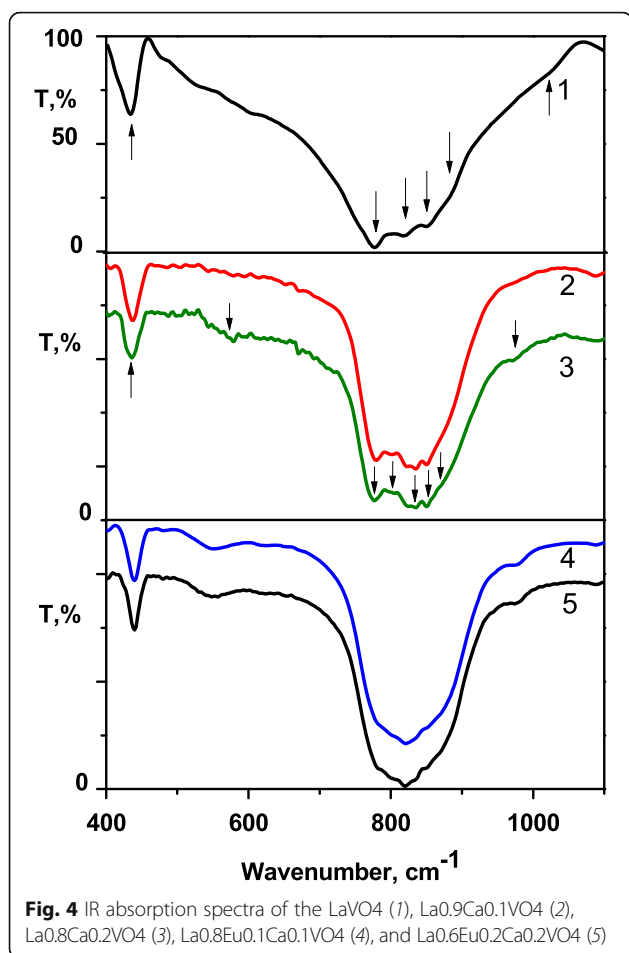
Analysis of data presented in Table 1 gives possibility to note the next.

1. Data of the SEM experiments on the contents of the La^{3+} ions in the synthesized samples (first column of the Table 1) are quite closed to the expected compositions (see the far right column of the Table 1).
2. If we take the total content of the Eu^{3+} and Ca^{2+} ions, it is easy to see that the experimentally measured data are quite close to the expected

compositions. However, it is easy to see that the predicted simultaneous fourfold increase of ions Eu^{3+} and Ca^{2+} content (from 0.05 up to 0.20 at.%) is not implemented for the actual synthesized samples. We can observe when the content of the Eu^{3+} ions increases by ~10 times, the content of the Ca^{2+} ions

Table 1 Calculated starting composition of the La, Ca, and Eu atoms in the samples under synthesis, average content of atoms (in at.%), and evaluated composition of the synthesized samples

Starting composition	La	Eu	Ca	Evaluated composition
$La_{0.8}Ca_{0.2}$	41.2	–	9.4	$La_{0.81}Ca_{0.19}$
$La_{0.9}Eu_{0.05}Ca_{0.05}$	26.60	0.73	1.76	$La_{0.92}Eu_{0.02}Ca_{0.06}$
$La_{0.8}Eu_{0.10}Ca_{0.10}$	20.81	2.34	1.11	$La_{0.86}Eu_{0.10}Ca_{0.04}$
$La_{0.7}Eu_{0.15}Ca_{0.15}$	12.30	3.30	1.73	$La_{0.71}Eu_{0.19}Ca_{0.10}$
$La_{0.6}Eu_{0.20}Ca_{0.20}$	12.88	7.07	2.97	$La_{0.56}Eu_{0.31}Ca_{0.13}$

Chukova *et al. Nanoscale Research Letters* (2017) 12:340

Page 5 of 11

Fig. 4 IR absorption spectra of the LaVO4 (*1*), La0.9Ca0.1VO4 (*2*), La0.8Ca0.2VO4 (*3*), La0.8Eu0.1Ca0.1VO4 (*4*), and La0.6Eu0.2Ca0.2VO4 (*5*)

increases only by ~2–3 times. This is due both to specific of the samples (heterogeneity of sizes, shapes, and thickness of grains of powder, etc.) and features of the method (a significant error for light elements, the effect of electron beam on oxide surfaces, etc.). Nevertheless, this result should be taken into account when describing other properties of the synthesized compounds. First of all, it concerns their luminescent properties. To avoid misunderstanding, we will not change following designation of samples noted in the "Synthesis"
and "X-ray Diffraction" sections.

IR Spectroscopy

IR spectroscopy study of the $La_{1-x}Ca_xVO_4$ and $La_{1-x-y}Eu_yCa_xVO_4$ $(0 \leq x, y \leq 0.2)$ samples was performed to confirm their structure and composition. The view of the IR spectra in the range of 400–1100 cm^{-1} (Fig. 4) is typical for the LaVO$_4$ IR absorption spectra previously measured in this range [28–30]. These spectra are also very similar to the IR spectra of other lanthanide orthovanadates LnVO$_4$ (Ln = Y, Ce–Yb) [28, 31], multi-metal orthovanadates such as $M_3Ln(XO_4)_2$ and $M_2M'Ln(XO_4)_2$ (M, M' = Na, K, Rb) [32] and vanadates of the $M''_3V_2O_8$ (M'' = Mg, Ca, Sr, Ba, and Zn) type [33–35]. Namely, the spectra are similar to all of compounds; those lattices are built by isolated tetrahedral VO$_4^{3-}$ molecular groups.

It is well known that the bending (v_2 and v_4) and stretching vibrations (v_1 and v_3) of O–V–O bonds of the VO$_4^{3-}$ anion form IR absorption spectra of various orthovanadates in the range 400–700 and 700–1100 cm^{-1}, respectively [36, 37]. In fact, measured by us, spectrum of the undoped LaVO$_4$ contains separated weak bands located in the range 400–700 cm^{-1}, while stronger wide band lies in the range 700–1100 cm^{-1} (Fig. 4, curve 1). Sharp peak at 434 cm^{-1} and blurred band centered near 550 cm^{-1} compose IR spectra of this sample in the former range. The main peak at ~778 cm^{-1} and three strongly overlapped other ones located at ~820, 850, and 880 cm^{-1} form wide band (Fig. 4, curve 1). (All the mentioned peaks are marked by arrows close to the curve 1 in Fig. 4, and their positions are in Table 2).

When LaVO$_4$ is doped by the Ca^{2+} ions, the shapes of spectral bands and peaks positions are changed, but these changes are not as striking as one could expect, but we should note that composition of peaks changes. As a result, six peaks marked by arrows can be found on the curves 2 and 3 of Fig. 4 in the range of wide absorption band.

Table 2 IR peaks positions (in cm^{-1}) and their attributions to vibration modes in the VO$_4^{3-}$ vanadate groups

LaVO$_4$	La$_{0.9}$Ca$_{0.1}$VO$_4$	La$_{0.8}$Ca$_{0.2}$VO$_4$	La$_{0.8}$Eu$_{0.1}$Ca$_{0.1}$VO$_4$	La$_{0.6}$Eu$_{0.2}$Ca$_{0.2}$VO$_4$	Vibration modes
434	438	436	439	440	v_4
	570	553	553		
778	780	777	783	780	
	802	801	802	801	
				811	v_3
820	822	824	821	820	
850	836; 850	835; 850	835; 854	836; 852	
880	874	875	875	874	v_1
1026	976	975	918; 978	975	

Chukova *et al. Nanoscale Research Letters* (2017) 12:340

Page 6 of 11

If the Eu^{3+} ions are added to the $La_{1-x}Ca_xVO_4$ compounds, then band of stretching vibrations becomes more complicated and its components are more overlapped (Fig. 4, curves 4 and 5). Thus, six or seven peaks can be distinguished there (see arrows), and shape and structure of the band become very similar to ones previously published on IR absorption spectra of the $LaVO_4$ containing Eu^{3+} ions [31, 36]. (The peaks positions of all measured IR absorption bands are accumulated in Table 2.)

The exact assignment of spectral components to a certain type of modes is difficult, especially that concerns stretching vibration range. Due to the low C_s symmetry of the VO_4^{3-} molecular anion in monoclinic $LaVO_4$, four IR lines lying close to each other can appear in this range of spectra. Our experimental findings are in good agreement with noted above theoretical prediction. Mentioned fact causes strong overlapping of the lines, that is why they are revealed as one complex wide band. Doping with calcium ions causes a distortion of certain amount of vanadates groups. As a result, additional peaks appear in the spectrum. Besides, as we have shown above, all co-doped samples under our study are a mixture of monoclinic and tetragonal $LaVO_4$ phases and contribution of the phases depends on the dopant concentration. The VO_4^{3-} molecular groups possess D_{2d} symmetry in tetragonal $LaVO_4$. So, two lines of E_u and A_{2u} symmetry can be found in the range of stretching vibrations if morphology of the VO_4^{3-} groups corresponds to ideal tetragonal lattice structure. Really, neighbor environment and symmetry of some VO_4^{3-} groups in tetragonal lattice are also deformed by Ca^{2+} ions, and all of VO_4^{3-} internal vibrations can occur in the IR spectra. As previously have been reported, the calculated [38] and measured [31] peak positions of the IR absorption lines for tetragonal $LaVO_4$ are close to those for monoclinic $LaVO_4$. Thus, the eight lines can form the range of stretching vibrations, we suppose. Change of the phase composition leads to mentioned changes of the shape of the IR bands and their positions. Regarding published theoretical and experimental data, a possible assignment of all measured features was made (Table 2). Additional studies are necessary in order to clarify the origin of the bands that are in the ranges 500–700 and 900–1000 cm^{-1}. We can only note that similar features were previously observed in the IR absorption spectra of some Ca containing orthovanadates [33, 34].

In any cases, we are able to state that observed IR spectra confirm that anionic sub-lattice of studied vanadates is built by VO_4^{3-} molecular anions.

Luminescent Spectroscopy

Emission of the $La_{1-x}Ca_xVO_4$ samples is observed in a wide spectral range from 400 to 800 nm. The observed bands are complex. The photoluminescence (PL) spectra contain two wide and strongly overlapped components at position of their maximum near ~570 and ~630 nm (Fig. 5). The band positions and structure of the spectra are similar to those described previously as for undoped nanosized $LaVO_4$ and $Ba_3V_2O_8$ compounds, as well as for activated $Sr_{2.91}V_2O_8$:0.06Eu^{3+}, $Ca_2NaMg_2V_3O_{12}$:Eu^{3+}, and $Na_2LnMg_2V_3O_{12}$ vanadate phosphors [17, 21, 39, 40]. The observed bands can be assigned to electron transitions in the VO_4^{3-} groups; those are constituents of mentioned compounds. The charge transfer transitions of 3d orbitals electron of the V^{5+} ion to the 2p orbital electron of the O^{2-} ion inside of the VO_4^{3-} groups are the nature of this luminescence [40, 41]. According to energy scheme of the vanadate tetrahedron, emission bands at 570 and 630 nm are connected respectively with $^3T_2$ and $^3T_1 \rightarrow$ $^1A_1$ electron transitions in the VO_4^{3-} groups [39–41]. These transitions are forbidden in the ideal T_d symmetry of the VO_4^{3-} group. Distortion of the VO_4^{3-} tetrahedrons from the ideal symmetry in the crystal lattice of $LaVO_4$ enhances the spin–orbit interaction and makes these transitions partially allowed [42]. As we noted above, in the monoclinic phase of the $La_{1-x}Ca_xVO_4$ samples, the VO_4^{3-} groups have distorted symmetry. Besides, some of these groups are affected by Ca^{2+} ions. The VO_4^{3-} group also is of lower symmetry than T_d in tetragonal $La_{1-x-y}Eu_y$-Ca_xVO_4 samples. Thus, we have all the reasons to assign the observed 570 and 630 nm bands to the $^3T_2$ and $^3T_1 \rightarrow {}^1A_1$ electron transitions in the VO_4^{3-} groups.

Emission of the $La_{1-x-y}Eu_yCa_xVO_4$ samples is observed in the 550–730 nm spectral range and consists of narrow spectral lines, and undoubtedly, they are caused by radiation transitions in Eu^{3+} ions (Figs. 6 and 7). The emission intensity increases if content of dopants increases in the range $(0 \leq x \leq 0.15)$ (Fig. 7).

Excitation spectra of all the synthesized samples are typical for luminescence excitation spectra of undoped and doped with Eu^{3+} ions $LaVO_4$ [20–23, 42–44]. They
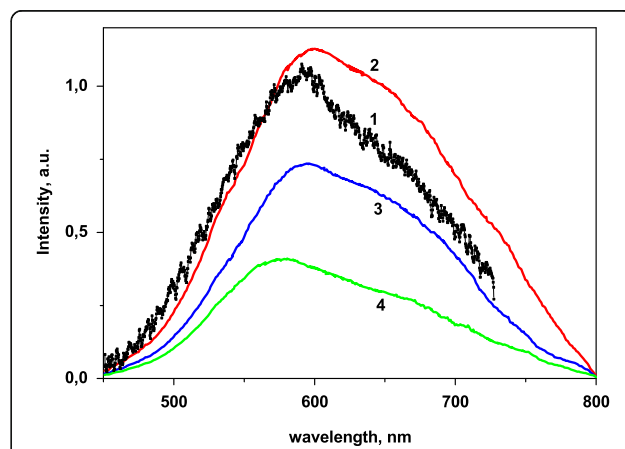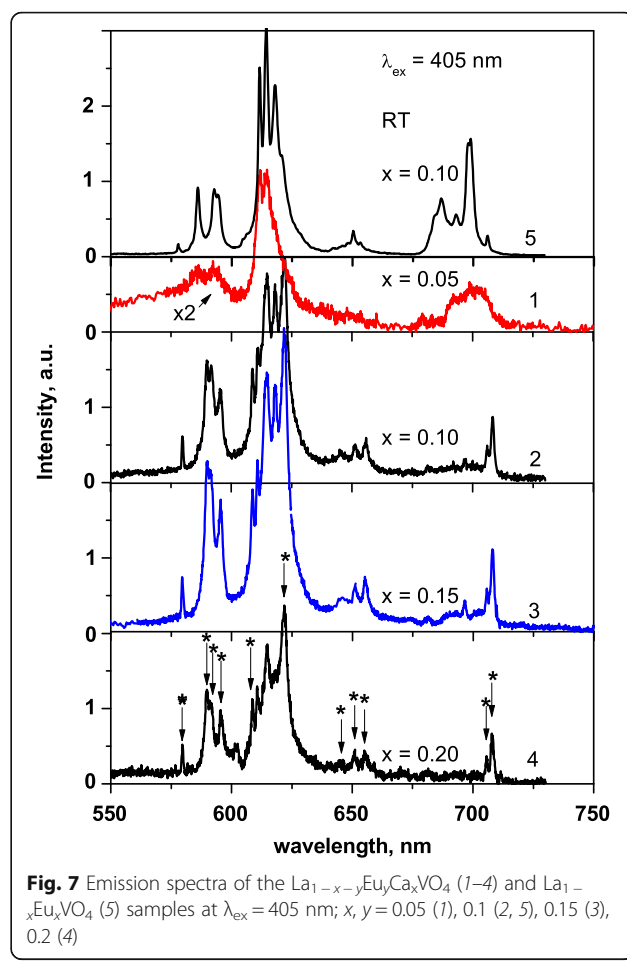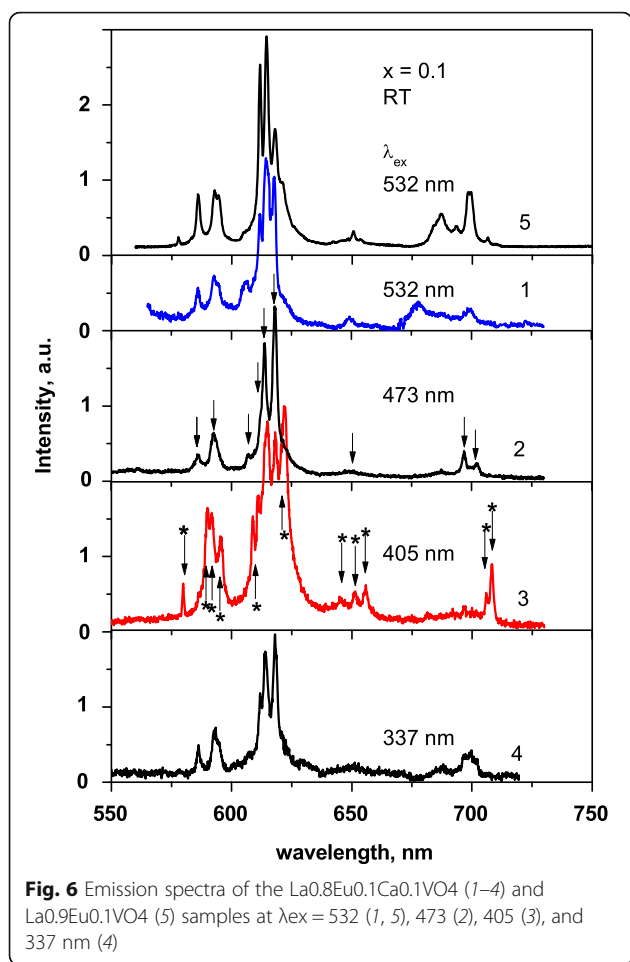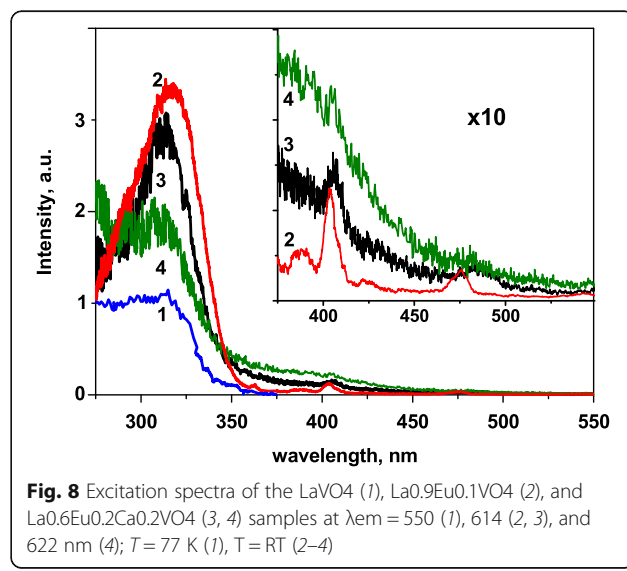

Fig. 5 Emission spectra of the $La_{1-x}Ca_xVO_4$ samples, $\lambda_{ex} = 310$ (*1–3*) and 290 nm (*4*); x = 0 (*1*), 0.2 (*2*), and 0.1 (*3, 4*), $T = 77$ K

Chukova *et al. Nanoscale Research Letters* (2017) 12:340

Page 7 of 11

Fig. 6 Emission spectra of the La0.8Eu0.1Ca0.1VO4 (*1–4*) and La0.9Eu0.1VO4 (*5*) samples at λex = 532 (*1, 5*), 473 (*2*), 405 (*3*), and 337 nm (*4*)

Fig. 7 Emission spectra of the $La_{1-x-y}Eu_yCa_xVO_4$ (*1–4*) and $La_{1-x}Eu_xVO_4$ (*5*) samples at λex = 405 nm; *x*, *y* = 0.05 (*1*), 0.1 (*2, 5*), 0.15 (*3*), 0.2 (*4*)

contain wide band with peak position at about 320 nm (Fig. 8). Also, two narrow weak peaks at ~405 and ~475 nm are presented in the spectra of the Eu-containing samples.

Structure of the emission spectra depends on the excitation wave length, λ_{ex} (Fig. 6), and on the concentration of the Ca^{2+} and Eu^{3+} dopants (Fig. 7). For the $La_{0.8}Eu_{0.1}Ca_{0.1}VO_4$ sample, which is just a mixture of monoclinic and tetragonal phases (see Fig. 2), the PL lines at 586, 592.5, 607, 611, 614, 618, 649, 697, and 702 nm (marked by arrows at Fig. 6, curve 2) are observed at all applied λ_{ex}. (*We call this set of the lines as first set.*) Note also that the ratio of intensity of the lines at 611, 614, and 618 nm changes if λ_{ex} varies. Besides, intensive lines at 580, 590, 591.7, 595.6, 608.7, and 622 and lines near 645, 651, 655, 706, and 708 nm (marked by arrows with asterisk at Fig. 6, curve 3, and at Fig. 7, curve 4) are distinctively observed in the spectra measured at λ_{ex} = 405 nm. (*We call this set of the lines as second set.*) So, the measured emission spectra are the superposition of two sets of luminescence lines. Since we have shown above that the sample $La_{0.8}Eu_{0.1}Ca_{0.1}VO_4$ is just a mixture of two crystalline phases, we have first to suppose

Fig. 8 Excitation spectra of the LaVO4 (*1*), La0.9Eu0.1VO4 (*2*), and La0.6Eu0.2Ca0.2VO4 (*3, 4*) samples at λem = 550 (*1*), 614 (*2, 3*), and 622 nm (*4*); *T* = 77 K (*1*), T = RT (*2–4*)

that these sets are related with emission of Eu^{3+} centers in monoclinic and tetragonal phases.

With the intent to clarify this assumption, we performed study of the luminescence spectra dependence on the samples composition at the same excitation wave length, $\lambda_{ex} = 405$ nm (Fig. 7). We found that the emission spectra of the samples where $x = 0.1$ and 0.15 are very close to each other (Fig. 7, curves 3 and 4). This finding agrees with the statement that these samples are the mixture of two phases. Tetragonal phase dominates in the $La_{0.6}Eu_{0.2}Ca_{0.2}VO_4$ sample, and we see that *second set of the luminescence lines also* dominates in the spectrum of this sample, but we see also that mentioned before line at 618 nm is vanished in this spectrum (Fig. 7, curve 4). When observe the emission spectrum of the $La_{0.9}Eu_{0.05}Ca_{0.05}VO_4$ (Fig. 7, curve 1), we see that *first set of lines* mainly reveals in the spectrum (Fig. 7, curve 1). As the $La_{0.9}Eu_{0.05}Ca_{0.05}VO_4$ sample is monoclinic (see Fig. 2), we should relate the *first set* of lines to emission of Eu^{3+} ions in monoclinic crystal phase. At the same time, we note that line at 618 nm is also vanished in this spectrum. So, we concluded that not only competition between content of the crystal phases influence luminescence behavior. Let us discuss the question in detail.

The observed narrow PL lines are caused by the $^5D_0 \rightarrow {}^7F_J$ (J = 0, 1, 2, 3, 4) electron radiation transitions in the inner $4f^n$ shell of the Eu^{3+} ions. The ^7F_J energy levels may be split in the crystal field on the $2j + 1$ sub-levels, but some of possible transitions can be forbidden by the symmetry rules [45]. If the Eu^{3+} ions occupy the site of the La^{3+} ions in tetragonal $LaVO_4$ crystal lattice (I41/amd space group), they have D_{2d} site symmetry. In such a case, group theory predicts no luminescence peaks from $^5D_0 \rightarrow {}^7F_0$ transition, two lines from the $^5D_0 \rightarrow {}^7F_1$ and three lines from the $^5D_0 \rightarrow {}^7F_2$ transitions. If the Eu^{3+} ions occupy the site of the La^{3+} ions in monoclinic $LaVO_4$ crystal lattice (P2$_1$/n space group), they have C_1 site symmetry. In this case, group theory predicts manifestation all of possible transitions: one luminescence peak from the $^5D_0 \rightarrow {}^7F_0$ transition, three lines from $^5D_0 \rightarrow {}^7F_1$ and five lines from the $^5D_0 \rightarrow {}^7F_2$ transitions [44].

So, it was not surprising that accounting the spectra in Fig. 6 in sum, we have found one line for the $^5D_0 \rightarrow {}^7F_0$ (spectral range 570–585 nm), five lines (586, 592.5, 590, 591.7, 595.6 nm) for the $^5D_0 \rightarrow {}^7F_1$ (spectral range 585–600 nm), and seven lines (607, 614, 618, 608.7, 611, 614, 622 nm) for $^5D_0 \rightarrow {}^7F_2$ transitions (spectral range 600–650 nm), as this figure shows the luminescence spectra of the sample which is mixture of the monoclinic and tetragonal phases. This statement also concerns the spectra 2 and 3 in Fig. 7, as they also represent luminescence of the mixture, $x = 0.1$ and 0.15, respectively. It was surprising that we see intensive line from the $^5D_0 \rightarrow {}^7F_0$ transition for the $La_{0.6}Eu_{0.2}Ca_{0.2}VO_4$ sample which represents only

tetragonal crystal structure (Fig. 7, curve 4). Moreover, we see that the spectrum of the monoclinic $La_{0.9}Eu_{0.05}Ca_{0.05}VO_4$ sample (Fig. 7, curve 1) is lesser complicated than it might be expected to this structure. At the same time, it is important that luminescence intensity of these samples is lower if compared to intensity for other samples shown in this Figure. As we go from spectrum 1 to spectrum 4 in Fig. 7, the contribution of monoclinic phase decreases. These results mean that other factors, not only crystal structure, significantly determine luminescence behavior of the samples under study. Thus, we supposed that as shown in Figs. 6 and 7, curves 2–4, spectral transformations are mainly related to luminescence behavior of tetragonal phase, especially to role of Ca^{2+} cations, as their concentration increases by 2–3 times when gone from $x = 0.1$ to 0.2 (see the "Morphology and Chemical Element analysis" section).

In fact, obtained results mean that at least two of different type luminescence centers formed by the ions Eu^{3+} in the sample of tetragonal structure contribute to the PL spectra. We ascribed the abovementioned spectral lines to emission of type I ("first set" of lines) and type II of the centers ("second set" of lines). Emission line from the $^5D_0 \rightarrow {}^7F_0$ transition (580 nm) is observed only for the type II centers, and the most intensive lines of the $^5D_0 \rightarrow {}^7F_2$ and $^5D_0 \rightarrow {}^7F_4$ transitions for these centers are located at 622 and 708 nm, respectively. For type I centers, the most intensive lines are located at 614 and 697 nm. These spectral features allow us to do assumption that types I and II of centers are characterized by different symmetry of the Eu^{3+} ions environment: the type I centers are characterized by higher site symmetry and the type II centers are characterized by lower site symmetry in the crystal lattices [45]. We supposed that type I centers are formed by the Eu^{3+} ions in their regular positions in the crystal lattice (D_{2d} symmetry).

As for the type II centers, we suppose that they can be formed by Eu^{3+} ions disturbed by defects generated as a result of Ca^{2+} cations incorporation into $LaVO_4$ crystal lattice. To confirm this supposition, we performed additive experimental study of the sample that does not contain Ca^{2+} ions, namely, $La_{0.9}Eu_{0.1}VO_4$ composition of tetragonal structure [14, 23] (Figs. 6 and 7, curves 5). Taking into account that above noted lines of type II centers (e.g., lines at 622 and 708 nm) were not observed for the Ca^{2+}-free sample (Fig. 7, curve 5), we concluded that the most possible origin of the type II centers is the Eu^{3+} ions disturbed by Ca-induced defects. In the case of the doped with calcium $LaVO_4$ lattice, the Ca^{2+} dopant has to replace the La^{3+} ions. Then, effective "–1" charge arises. Charge compensation of mentioned –1 charge is needed, as the crystal has to be electro-neutral. This compensation can be achieved via formation of one oxygen vacancy, $[V_O]^{2+}$, on each two Ca^{2+}/La^{3+}

Chukova *et al. Nanoscale Research Letters* (2017) 12:340

Page 9 of 11

replacements. Thus, for the Ca^{2+} dopants arrangement in the $LaVO_4$ crystal lattice, we should expect that some of the Eu^{3+} ions are under the effect of both neighbor Ca^{2+} cations and oxygen vacancy. Thus, we can assume that such Eu^{3+} ions are just the type II of the luminescence centers, and their local symmetry is lower if comparing to symmetry of the type I centers. Taking into account that $^5D_0 \rightarrow {}^7F_0$ transition emission line (near 580 nm) is observed in the spectra (Figs. 6 and 7), the symmetry of type II centers may be C_2 or C_s [44, 45]. The C_2 symmetry of the Eu^{3+} surrounding in the I41/amd space group of orthovanadates can be achieved only by equal distortions of two oxygen positions. Therefore, we assume that case of the C_s symmetry of the Eu^{3+} surrounding at the type II centers is more probable.

Excitation spectra measured in the emission lines corresponded to different types of centers (614 and 622 nm for types I and II centers, respectively) confirmed made above description, as these spectra revealed some differences (Fig. 8). The wide band at 320 nm is more intensive in the excitation spectra of type I centers. The 320-nm band is also observed in the spectra of the $La_{0.9}Eu_{0.1}VO_4$ sample (Fig. 8, curve 2). This band is caused by electron transitions in the vanadate VO_4^{3-} groups. Therefore, the type I centers are better excited through the matrix than type II centers, that confirms our assumptions about relation of the type I centers with the Eu^{3+} ions in the regular positions in the crystal lattice.

Total emission intensity of the $La_{1-x-y}Eu_yCa_xVO_4$ samples have shown essential increasing when dopant concentration increases up to $x, y = 0.15$ (Fig. 9, curve 1). Similar dependence reveal peak intensity of the 614 and 622 nm lines caused by luminescence of types I and II centers, respectively (Fig. 9, curve 2 and 3), but we see that main contribution to luminescence enhance is related with emission of type II of centers. Therefore, spectral behavior of the type II luminescence centers is not only single

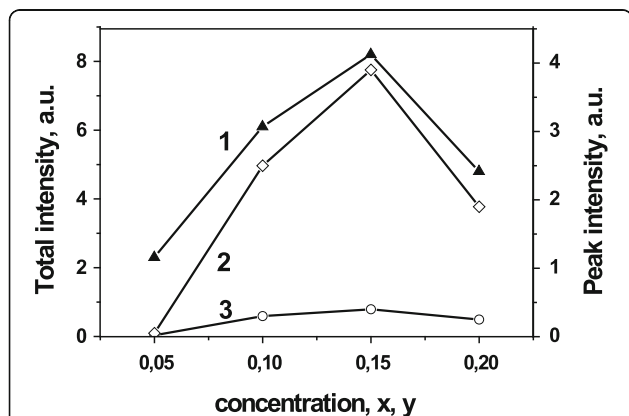**Fig. 9** Dependencies of the $La_{1-x-y}Eu_yCa_xVO_4$ luminescence intensity on dopant concentration x; total emission (*1*) and 622 nm peak intensity (*2, 3*); λex = 405 (*1, 2*) and 473 nm (*3*)

manifestation of the Ca^{2+} cations influence on the $La_{1-x-y}Eu_yCa_xVO_4$ emission. The Ca^{2+} doping enhances also efficiency of this type of luminescence centers.

As for quenching of the luminescence intensity at $x, y > 0.15$, it should be noted that several mechanisms may be responsible for this. First, it is concentration quenching related with Eu^{3+} content. Then, as we described in the "Morphology and Chemical Element Analysis" section, the sizes of particle decreases for the $La_{0.6}Eu_{0.2}Ca_{0.2}VO_4$ sample. So, the surface quenching can be important mechanism in this case.

Surely, made assumption about role of the Ca^{2+} ions in luminescence of the lanthanum vanadate, $LaVO_4$, co-doped with Eu^{3+} and Ca^{2+} ions requires additional study, and we plan to carry out it in the future.

Conclusions

The $La_{1-x}Ca_xVO_4$ and $La_{1-x-y}Eu_yCa_xVO_4$ ($0 \le x, y \le 0.2$) micro/nanosized powders were prepared by aqueous nitrate–citrate sol–gel synthesis. Phase composition of the sample depends on the x and y values.

The $La_{0.9}Ca_{0.1}VO_4$ is crystallized in monoclinic structure up to the $x = 0.1$.

The $La_{0.9}Eu_{0.05}Ca_{0.05}VO_4$ sample was also attributed to the monoclinic structure.

Increasing concentration of europium, Eu^{3+}, and calcium ions, Ca^{2+}, in $La_{1-x-y}Eu_yCa_xVO_4$ solid solutions leads to the change of the crystal structure, and subsequently, stabilization of the tetragonal phase takes place.

Phase transformation and especially Ca^{2+} ions influence IR spectroscopy and luminescence behavior of studied compounds, as Ca^{2+} ions impact both on VO_4^{3-} molecular groups and La^{3+} and Eu^{3+} ions.

Emission of the $La_{1-x}Ca_xVO_4$ samples consists of wide bands in the 450–800 nm spectral range. These bands were ascribed to electron transitions in the distorted VO_4^{3-} vanadate groups.

Emission of the $La_{1-x-y}Eu_yCa_xVO_4$ samples is observed in the 550–730 nm spectral range, and it consists of narrow spectral lines. These lines are caused by the $^5D_0 \rightarrow {}^7F_J$ electron transitions in the Eu^{3+} ions. The Eu^{3+} ions form two types of emission centers in the samples under study. The assumption was made that type I centers are formed by the Eu^{3+} ions in their regular positions in the crystal lattice, while the type II centers have complex structure and they consists of Eu^{3+} ions, Ca^{2+} cations, and oxygen vacancies.

Chukova *et al. Nanoscale Research Letters* (2017) 12:340

Page 10 of 11

Authors' Contributions
SN contributed to the development of strategy of the work and its scientific management, luminescent SEM study, and processing and discussion of the measurement results. OCh contributed to the luminescent spectra measurements, processing and analysis of taken results, and discussion of luminescence and IR spectroscopy results. SAN contributed to the development of strategy of the chemical part of this work and its scientific management, synthesis adjustment, and analysis of IR spectroscopy and XRD results. AS contributed to the solution for synthesis and samples' preparation, IR spectroscopy measurement and processing of measurement results, XRD study, and processing and analysis of their results. TV contributed to the study, analysis, and discussion of the synthesis results, IR spectroscopy and XRD study, and discussion of the measurement results. All authors read and approved the final manuscript.

Competing Interests
The authors declare that they have no competing interests.

Publisher's Note
Springer Nature remains neutral with regard to jurisdictional claims in published maps and institutional affiliations.

Author details
[1]Faculty of Physics, Taras Shevchenko National University of Kyiv, 64/13, Volodymyrska Str, 01601 Kyiv, Ukraine. [2]Faculty of Chemistry, Taras Shevchenko National University of Kyiv, 64/13, Volodymyrska Str, 01601 Kyiv, Ukraine.

References

1. Li W, Li D, Lin Y, Wang P, Chen W, Fu X, Shao Y (2012) Evidence for the active species involved in the photodegradation process of methyl orange on TiO_2. J Phys Chem 116(5):3552–3560
2. Shen J, Sun L-D, Yan C-H (2008) Luminescent rare earth nanomaterials for bioprobe applications. Dalton Trans 42(14):5661–5808
3. Huse M, Norby T, Haugsrudz R (2011) Proton conductivity in acceptor-doped $LaVO_4$. J Electrochem Soc 158(8):B857–B865
4. Lin H-Y, Chang W-F, Chu S-Y (2013) Luminescence of (Ca, Sr)3(VO4)2:Pr3+, Eu3 + phosphor for use in CuPc-based solar cells and white light-emitting diodes. J Lumin 133:194–199
5. Zhang Y, Li G, Yang X, Yang H, Lu Z, Chen R (2013) Monoclinic $BiVO_4$ micro-/nanostructures: microwave and ultrasonic wave combined synthesis and their visible-light photocatalytic activities. J Alloys Compd 551:544–550
6. Wang D, Li R, Zhu J, Shi J, Han J, Zong X, Li C (2012) Photocatalytic water oxidation on $BiVO_4$ with the electrocatalyst as an oxidation cocatalyst: essential relations between electrocatalyst and photocatalyst. J Phys Chem 116(8):5082–5089
7. Garg AB, Errandonea D (2015) High-pressure powder X-ray diffraction study of $EuVO_4$. J Solid State Chem 226:147–153
8. Cheng X, Guo D, Feng S, Yang K, Wang Y, Ren Y, Song Y (2015) Structure and stability of monazite- and zircon-type $LaVO_4$ under hydrostatic pressure. Opt Mater 49:32–38
9. Tamilmani V, Sreeram KJ, Nair BU (2015) Catechin assisted phase and shape selection for luminescent $LaVO_4$ zircon. RSC Adv 5(100):82513–82523
10. Mialon G, Gohin M, Gacoin T, Boilot J-P (2008) High temperature strategy for oxide nanoparticle synthesis. ACS Nano 2(12):2505–2512
11. Venkataraman BV, Sudha S (2005) Vanadium Toxicity. Asian J Exp Sci 19(2):127–134
12. Clark AS, Fagant JM, Mitch WE (1985) Selectivity of the insulin-like actions of vanadate on glucose and protein metabolism in skeletal muscle. Biochem J 232:273–276
13. Tyminski A, Grzyb T, Lis S (2016) REVO4-based nanomaterials (RE = Y, La, Gd, and Lu) as hosts for Yb3+/Ho3+, Yb3+/Er3+, and Yb3+/Tm3+ ions: structural and up-conversion luminescence studies J Am Ceram Soc (Article in Press)
14. Chornii V, Chukova O, Nedilko SG, Nedilko SA, Voitenko T (2016) Enhancement of emission intensity of $LaVO_4$:RE3+ luminescent solar light absorbers. Phys Status Solidi C 13(1):40–46
15. Nedilko SG, Chornii V, Chukova O, Degoda V, Bychkov K, Terebilenko K, Slobodyanik M (2016) Luminescence properties of the new complex La, BiVO4: Mo, Eu compounds as materials for down-shifting of VUV–UV radiation. Radiat Meas 90:282–286
16. Qin C, Huang Y, Seo H (2013) Structure and luminescence of new red-emitting materials-Eu3+-doped triple orthovanadates NaALa(VO4)2 (A = Ca, Sr, Ba). J Am Ceram Soc 96:1181–1187
17. Yoon SJ, Park K (2014) Synthesis and photoluminescent properties of white-emitting Sr2.91V2O8:0.06Eu3+ phosphors. Op Mater 36:1305–1310
18. Ardanova LI, Chukova OV, Getman EI, Marchenko VI, Nedilko SG, Scherbatskyi VP (2002) Luminescent properties of the Ca5(VO4)3OH apatites with the heterovalence calcium replacement on alkali and rare-earth elements. Funct Mater 9(2):326–331
19. Chukova O, Nedilko S, Moroz Z, Pashkovskyi M (2003) Luminescence of the samarium ions doped in the complex oxides with heterovalence substitution. J Lumin 102–103:498–503
20. Shinde KN, Singh R, Dhoble SJ (2014) Photoluminescent characteristics of the single-host white-light-emitting Sr3-3x/2(VO4)2:xEu (0 < x < 0.3) phosphors for LEDs. J Lumin 146:91–96
21. Park KC, Mho S (2007) Photoluminescence properties of Ba3V2O8, Ba3(1−x)Eu2xV2O8 and Ba2Y2/3V2O8:Eu3+. J Lumin 122–123:95–98
22. Tian L, Mho S (2007) Enhanced photoluminescence of YVO4:Eu3+ by codoping the Sr2+, Ba2+ or Pb2+ ion. J Lumin 122–123:99–103
23. Chukova O, Nedilko SA, Nedilko SG, Sherbatsky V, Voitenko T (2013) Comparable structural and luminescent characterization of the La1−xEuxVO4 solid solutions synthesized by solid state and co-precipitation methods. Solid State Phenom 200:186–192
24. Xu Z, Li C, Hou Z, Peng C, Lin J (2011) Morphological control and luminescence properties of lanthanide orthovanadate LnVO 4 (Ln = La to Lu) nano-/microcrystals via hydrothermal process. Cryst Eng Comm 13:474–482
25. Chumha N, Kittiwachana S, Thongtem T, Thongtem S, Kaowphong S (2014) Synthesis and characterization of $GdVO_4$ nanostructures by a tartaric acid-assisted sol–gel method. Ceram Int 40:16337–16342
26. Boyko R, Chukova OV, Gomenyuk OV, Nagornyi PG, Nedilko SG (2005) Origin of red luminescence of sodium titanium phosphate crystals contained chromium and titanium ions. Phys Stat Sol 2(1):712–715
27. Chukova O, Nedilko S, Scherbatskyi V (2010) Luminescent spectroscopy and structure of centers of the impurity Eu3+ ions in lead tungstate crystals. J Lumin 130(10):1805–1812
28. Liu J, Li Y (2007) Synthesis and self-assembly of luminescent Ln3+-doped $LaVO_4$ uniform nanocrystals. Adv Mater 19:1118–1122
29. Liu G, Duan X, Li H, Dong H (2009) Hydrothermal synthesis, characterization and optical properties of novel fishbone-like $LaVO_4$:Eu3+ nanocrystals. Mater Chem Phys 115:165–171
30. Von Escobar ME, Baran EJ (1978) Uber die tetragonale Modifikation von Lanthan-orthowanadat. Z Anorg Allg Chem 441:273–277
31. Fang ZM, Hong Q, Zhou ZH, Dai SJ, Weng WZ, Wan HL (1999) Oxidative dehydrogenation of propane over a series of low-temperature rare earth orthovanadate catalysts prepared by the nitrate method. Catalysis Letters 61:39–44
32. Rghioui L, Benarafa L, El Jastimi J, El Hajji A, Lorriaux A, Wallart F (2012) Vibrational spectra and force field studies of K1,125Rb1,875La(VO4)2 vanadate. J Mater Environ Sci 3(1):58–65
33. Baran EJ (1976) Die Schwingungsspektren von Ca3(VO4)2 und Ca,(AsO,). Z Anorg Allg Chem 497:131–136
34. Parhi P, Manivannan V, Kohl S, McCurdy P (2008) Synthesis and characterization of M3V2O8 (M = Ca, Sr and Ba) by a solid-state metathesis approach. Bull Mater Sci (India) 31(6):885–890
35. Siebert H (1954) Kraftkonstante und Strukturchemie. V Struktur der Sauerstoffsäuren Z Anorg Allg Chem 275:225–240
36. Nakamoto K (1963) Infrared spectra of inorganic and coordination compounds. Wiley, New York, p 410
37. Melvin L (1974) Symmetry principles in solid state and molecular physics. Wiley, New York, p 499
38. Sun L, Zhao X, Li Y, Li P, Sun H, Cheng X, Fan W (2010) First-principles studies of electronic, optical and vibrational properties of $LaVO_4$ polymorph. J Appl Phys 108(9):093519–10
39. Sobszyk M, Szymański D (2013) A study of optical properties of Sm3+ ions in α-Na3Y(VO4)2 single crystals. J Lumin 142:96–102

Chukova *et al. Nanoscale Research Letters* (2017) 12:340

Page 11 of 11

40. Chukova O, Nedilko SA, Nedilko SG, Voitenko T, Gomenyuk O, Sheludko V (2015) Study of temperature behavior of luminescence emission of $LaVO_4$ and $La_{1-x}Eu_xVO_4$ powders. Solid State Phenom 230:153–159

41. Song D, Guo C, Li T (2015) Luminescence of the self-activated vanadate phosphors $Na_2LnMg_2V_3O_{12}$ (Ln = Y, Gd). Ceram Int 41:6518–6524

42. Setlur AA, Comanzo HA, Srivatava AM, Beers WWJ (2005) Spectroscopic evaluation of a white light phosphor for UV-LEDs-$Ca_2NaMg_2V_3O_{12}$:Eu^{3+}. J Electrochem Soc 152(12):H205–H208

43. Tao ZX, Tsuboi TJ, Huang YL, Huang W, Cai PQ, Seo HJ (2014) Photoluminescence properties of Eu^{3+}-doped glaserite-type orthovanadates $CsK_2Gd(VO_4)_2$. Inorg Chem 53(8):4161–4168

44. Park SW, Yang HK, Chung JW, Chen Y, Moon BK, Cho BC, Jeon JH, Kim JH (2010) Photoluminescent properties of $LaVO_4$ Eu^{3+} by structural transformation. Physica B 405:4040–44

45. Wybourne BG (1965) Spectroscopic properties of ions in crystals. Wiley, New York, p 236